PHYSICAL REVIEW B **95**, 041201(R) (2017)

Quantum oscillations without magnetic field

Tianyu Liu, D. I. Pikulin, and M. Franz
Department of Physics and Astronomy, University of British Columbia, Vancouver, British Columbia, Canada V6T 1Z1
and Quantum Matter Institute, University of British Columbia, Vancouver, British Columbia, Canada V6T 1Z4
(Received 19 August 2016; revised manuscript received 21 October 2016; published 9 January 2017)

When the magnetic field B is applied to a metal, nearly all observable quantities exhibit oscillations periodic in $1/B$. Such quantum oscillations reflect the fundamental reorganization of electron states into Landau levels as a canonical response of the metal to the applied magnetic field. We predict here that, remarkably, in the recently discovered Dirac and Weyl semimetals, quantum oscillations can occur in the complete absence of magnetic field. These zero-field quantum oscillations are driven by elastic strain which, in the space of the low-energy Dirac fermions, acts as a chiral gauge potential. We propose an experimental setup in which the strain in a thin film (or nanowire) can generate a pseudomagnetic field b as large as 15 T and demonstrate the resulting de Haas–van Alphen and Shubnikov–de Haas oscillations periodic in $1/b$.

DOI: 10.1103/PhysRevB.95.041201

Dirac and Weyl semimetals [1–3] are known to exhibit a variety of exotic behaviors owing to their unusual electronic structure comprising linearly dispersing electron bands at low energies. This includes pronounced negative magnetoresistance [4–11] attributed to the phenomenon of the chiral anomaly [12–14], theoretically predicted nonlocal transport [15,16], Majorana flat bands [17], as well as unusual types of quantum oscillations (QOs) that involve both bulk and topologically protected surface states [18,19]. In this theoretical study we establish a mechanism for QOs in Dirac and Weyl semimetals that requires no magnetic field. These zero-field oscillations occur as a function of the applied elastic strain and, similar to the canonical de Haas–van Alphen and Shubnikov–de Haas oscillations [20], manifest themselves as oscillations periodic in $1/b$, where b is the strain-induced pseudomagnetic field, in all measurable thermodynamic and transport properties.

Materials with linearly dispersing electrons respond in peculiar ways to externally imposed elastic strain. In graphene, for instance, the effect of curvature is famously analogous to a pseudomagnetic field [21] that can be quite large and is known to generate pronounced Landau levels observed in tunneling spectroscopy [22]. Recent theoretical work [23–27] showed that similar effects can be anticipated in three-dimensional Dirac and Weyl semimetals, although the estimated field strengths in the geometries that have been considered are rather small (below 1 T in Ref. [26]). Ordinary quantum oscillations, periodic in $1/B$, have already been observed in the Dirac semimetals Cd_3As_2 and Na_3Bi [19,28–30] but the magnetic field required is $B \gtrsim 2$ T. This, then, would seem to rule out the observation of strain-induced QO in geometries considered previously. We make a key advancement in this Rapid Communication by devising a geometry in which a pseudomagnetic field b as large as 15 T can be achieved. The proposed setup consists of a thin film (or a nanowire) in which a pseudomagnetic field b is generated by a simple bend, as illustrated in Fig. 1.

For simplicity and concreteness we focus in the following on the Dirac semimetal Cd_3As_2 [28,31–35] which is the best characterized representative of this class of materials. Our results are directly applicable also to Na_3Bi [36–38], whose low-energy description is identical, and are easily extended to other Dirac and Weyl semimetals [39–44]. We start from the tight-binding model formulated in Refs. [31,36], which describes the low-energy physics of Cd_3As_2 by including the band inversion of its atomic Cd $5s$ and As $4p$ levels near the Γ point. In the basis of the spin-orbit-coupled states $|P_{\frac{3}{2}}, \frac{3}{2}\rangle$, $|S_{\frac{1}{2}}, \frac{1}{2}\rangle$, $|S_{\frac{1}{2}}, -\frac{1}{2}\rangle$, and $|P_{\frac{3}{2}}, -\frac{3}{2}\rangle$, the model is defined by a 4×4 matrix Hamiltonian

$$H^{\text{latt}} = \epsilon_{\boldsymbol{k}} + \begin{pmatrix} h^{\text{latt}} & 0 \\ 0 & -h^{\text{latt}} \end{pmatrix}, \tag{1}$$

on a simple rectangular lattice with spacings $a_{x,y,z}$, where

$$h^{\text{latt}}(\boldsymbol{k}) = m_{\boldsymbol{k}}\tau^z + \Lambda(\tau^x \sin a_x k_x + \tau^y \sin a_y k_y), \tag{2}$$

$\boldsymbol{\tau}$ are Pauli matrices in the orbital space, and $m_{\boldsymbol{k}} = t_0 + t_1 \cos a_z k_z + t_2(\cos a_x k_x + \cos a_y k_y)$. For the analytic calculations below we will assume $a_i = a$, while in numerics we will use the actual lattice constants of Cd_3As_2. Various tunneling amplitudes and $\epsilon_{\boldsymbol{k}}$ are given in the Supplemental Material (SM) [45]. The low-energy spectrum of h^{latt} consists of a pair of Weyl points, shown in Fig. 2(a), which carry opposite chirality $\eta = \pm 1$ and are located at crystal momenta

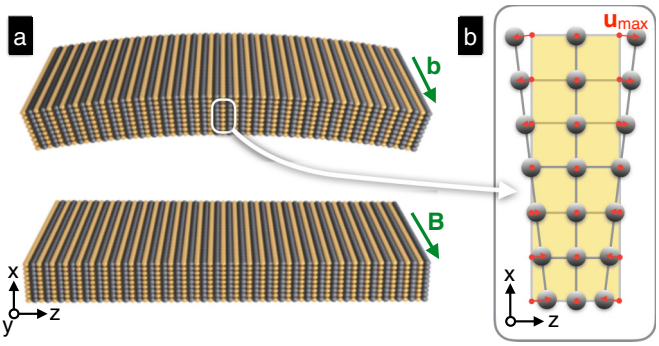

FIG. 1. Proposed setup for strain-induced quantum oscillation observation in Dirac and Weyl semimetals. (a) The bent film is analogous, in terms of its low-energy properties, to an unstrained film subject to magnetic field B. (b) Detail of the atomic displacements in the bent film. Displacements have been exaggerated for clarity.

$\boldsymbol{K}_\eta = (0,0,\eta Q)$, with Q given by $\cos(aQ) = -(t_0 + 2t_2)/t_1$. The lower diagonal block in Eq. (1) describes the spin-down sector in Cd_3As_2 and has an identical spectrum. Terms in $\epsilon_{\boldsymbol{k}}$ account for the particle-hole (p-h) asymmetry present in Cd_3As_2.

Following Refs. [23–26], the most important effect of elastic strain can be included in the lattice model (1) by modifying the electron tunneling amplitude along the $\hat{z}$ direction according to

$$t_1\tau^z \to t_1(1-u_{33})\tau^z + i\Lambda\sum_{j\neq 3} u_{3j}\tau^j, \tag{3}$$

where $u_{ij} = \frac{1}{2}(\partial_i u_j + \partial_j u_i)$ is the symmetrized strain tensor and $\boldsymbol{u} = (u_1,u_2,u_3)$ represents the displacement of the atoms. To see how this leads to an emergent vector potential, we study the low-energy effective theory by expanding $h^{\rm latt}(\boldsymbol{k})$ in the vicinity of the Weyl points $\boldsymbol{K}_\pm$. The low-energy Hamiltonian of the distorted crystal is derived in SM and reads

$$h_\eta(\boldsymbol{q}) = v_\eta^j\tau^j\left(\hbar q_j - \eta\frac{e}{c}\mathcal{A}_j\right), \tag{4}$$

with the velocity vector $\boldsymbol{v}_\eta = \hbar^{-1}a(\Lambda,\Lambda,-\eta t_1\sin aQ)$. For Cd_2As_3 parameters and lattice constant $a = 4$ Å, this gives $\hbar\boldsymbol{v}_\eta = (0.89,0.89,-1.24\eta)$ eV Å. The strain-induced gauge potential is given by

$$\vec{\mathcal{A}} = -\frac{\hbar c}{ea}(u_{13}\sin aQ, u_{23}\sin aQ, u_{33}\cot aQ). \tag{5}$$

We see that elements u_{j3} of the strain tensor act on the low-energy Weyl fermions as components of a chiral gauge field: $\vec{\mathcal{A}}$ couples with the opposite sign to the Weyl fermions with opposite chirality η. By contrast, the ordinary electromagnetic gauge potential couples with the same sign through the replacement $\hbar\boldsymbol{q} \to \hbar\boldsymbol{q} - \frac{e}{c}\boldsymbol{A}$. Reference [26] noted that the application of a torsional strain to a nanowire made of Cd_3As_2 (grown along the 001 crystallographic direction) results in a uniform pseudomagnetic field $\boldsymbol{b} = \nabla\times\vec{\mathcal{A}}$ pointed along the axis of the wire. The strength of this pseudomagnetic field was estimated as $b \lesssim 0.3$ T, which would be insufficient to detect QOs (although more subtle transport signatures related to the chiral anomaly should be observable [26]). Our key observation here is that a different type of distortion, illustrated in Fig. 1(a), can produce a much larger field b.

One reason why the torsion-induced b field is relatively weak lies in the fact that it originates from the $\mathcal{A}_x$ and $\mathcal{A}_y$ components of the vector potential. According to Eq. (5), these are suppressed relative to the strain components by a factor of $\sin aQ$. This is a small number in most Dirac and Weyl semimetals because the distance $2Q$ between the Weyl points is typically a small fraction of the Brillouin zone size $2\pi/a$. Specifically, we have $aQ \simeq 0.132$ in Cd_3As_2 [31]. Note, on the other hand, that the $\mathcal{A}_z$ component of the chiral gauge potential comes with a factor $\cot aQ \simeq 1/aQ$ and is therefore enhanced. A lattice distortion that produces a nonzero strain tensor element u_{33} will therefore be much more efficient in generating large b than u_{13} or u_{23}. Specifically, for the same amount of strain, the field strength is enhanced by a factor of $\cot aQ/\sin aQ \simeq 1/(aQ)^2 \simeq 57$ for Cd_3As_2. The physics of this pronounced asymmetry between the $\mathcal{A}_{x,y}$ and $\mathcal{A}_z$ components of the strain-induced gauge field can be traced back to the uniaxial anisotropy of the Cd_3As_2 band structure, which in turn stems from its layered crystal structure.

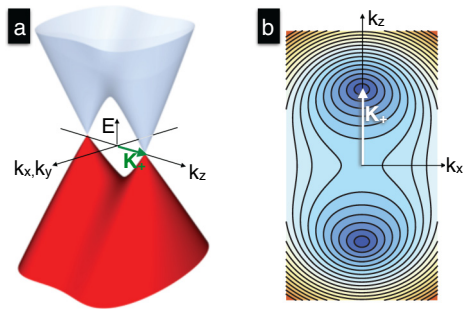

FIG. 2. Schematically shown low-energy electron excitation spectrum in Dirac and Weyl semimetals. (a) In a Dirac semimetal the bands are doubly degenerate due to the spin degree of freedom, while in a Weyl semimetal they are nondegenerate. (b) Contours of constant energy for $k_y = 0$. For magnetic field $\boldsymbol{B} \parallel \hat{y}$ these correspond to the extremal orbits [20] that give rise to QOs periodic in $1/B$.

To implement this type of strain, we consider a thin film (or a nanowire) grown such that vector $\boldsymbol{K}_\eta$ lies along the z direction, as defined in Fig. 1(a). More generally, we require that $\boldsymbol{K}_\eta$ has a nonzero projection onto the surface of the film or on the long direction of the nanowire. Cd_3As_2 films [29], microribbons [46], and nanowires [47,48] satisfy this requirement. Bending the film as shown in Fig. 1(b) creates a displacement field $\boldsymbol{u} = (0,0,2\alpha xz/d)$, where d is the film thickness and α controls the magnitude of the bend. (If R is the radius of the circular section formed by the bent film, then $\alpha = 2d/R$. α can also be interpreted as the maximum fractional displacement $\alpha = u_{\max}/a$ that occurs at the surface of the film.) This distortion gives $u_{33} = 2\alpha x/d$, which, through Eq. (5), yields a pseudomagnetic field

$$\boldsymbol{b} = \nabla\times\vec{\mathcal{A}} = \hat{y}\left(\frac{2\alpha}{d}\right)\frac{\hbar c}{ea}\cot aQ. \tag{6}$$

Noting that $\Phi_0 = hc/e = 4.12\times 10^5$ T Å, we may estimate the resulting field strength for a $d = 100$ nm film as

$$b \simeq \alpha\times 246\ \text{T}. \tag{7}$$

The maximum pseudomagnetic field that can be achieved will depend on the maximum strain that the material can sustain. Reference [47] characterized the Cd_3As_2 nanowires as "greatly flexible" and their Fig. 1(a) shows some wires bent with a radius R as small as several microns. This implies that α of several percent can likely be achieved. From Eq. (7) we thus estimate that a field strength of $b \simeq 10$–15 T can be reached, providing a substantial window for the observation of the strain-induced QOs.

To substantiate these claims we now present the results of our numerical simulations based on the lattice Hamiltonian (2). The magnetic field B is implemented via the standard Peierls substitution while the strain-induced field b through Eq. (3). The geometry outlined in Fig. 1 is used with periodic boundary conditions along y and z, open along x. Figure 3 provides the summary of our results. The unstrained crystal at zero field [Fig. 3(a)] shows the expected band structure with bulk Weyl

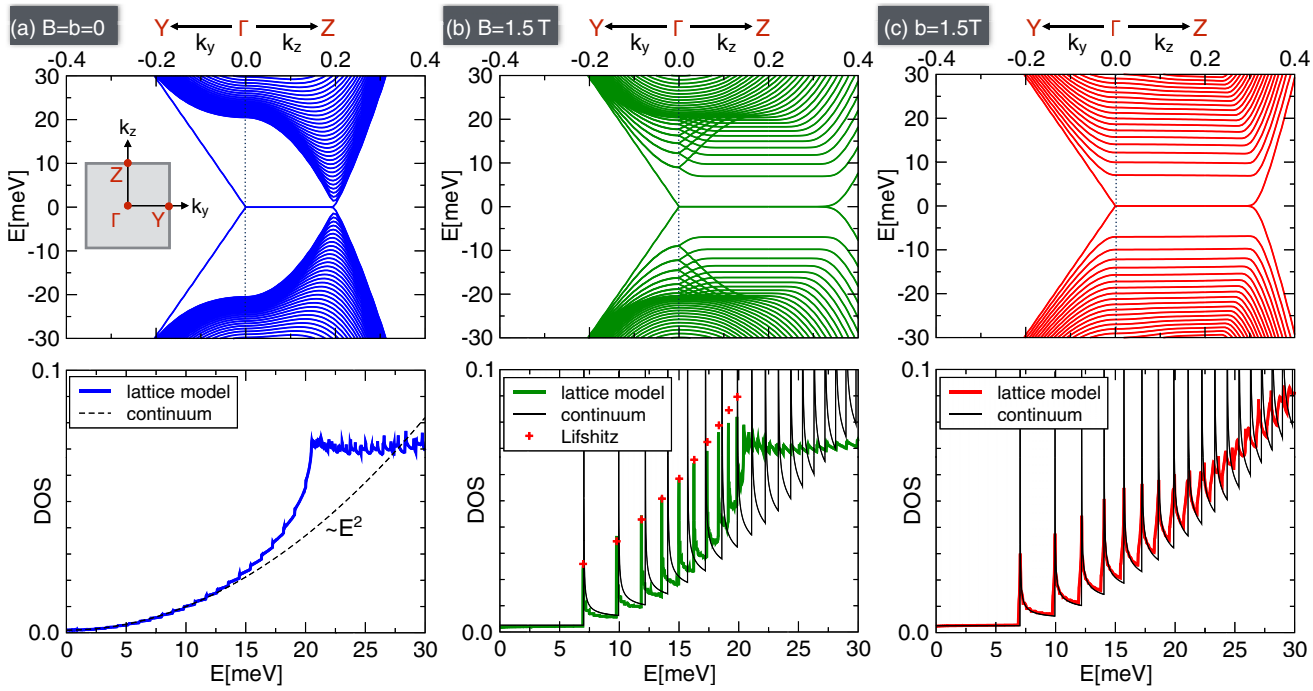

FIG. 3. Numerical results for the Cd_3As_2 lattice Hamiltonian. We model the Hamiltonian (2) in the presence of magnetic field $\boldsymbol{B} = \hat{y}B$ and strain-induced pseudomagnetic field $\boldsymbol{b} = \hat{y}b$. In all panels films of thickness 500 lattice points are studied with parameters appropriate for Cd_3As_2. The p-h asymmetry terms $\epsilon_{\boldsymbol{k}}$ are neglected for simplicity, which makes contributions from the two spin sectors identical. (a) Band structure and density of states (DOS) for zero field and zero strain. The inset shows the first Brillouin zone. (b) Band structure and normalized DOS for $B = 1.5$ T. Red crosses indicate the peak positions expected on the basis of the Lifshitz-Onsager quantization condition [20]. (c) Band structure and DOS for $b = 1.5$ T. The thin black line shows the expected bulk DOS for ideal Weyl dispersion computed from Eq. (8).

nodes close to $k_z a = \pm 0.2$ and a pair of linearly dispersing surface states corresponding to Fermi arcs. The density of states (DOS) exhibits the expected quadratic behavior $D(E) \sim E^2$ at low energies with some deviations apparent for $|E| \gtrsim 12$ meV due to the departure of the lattice model from the perfectly linear Weyl dispersion. At $E_{\mathrm{Lif}} \simeq 20$ meV a Lifshitz transition occurs where two small Fermi surfaces associated with each Weyl point merge into a single large Fermi surface, as illustrated in Fig. 2(b).

In Fig. 3(b) the magnetic field $\boldsymbol{B} = \hat{y}B$ is seen to reorganize the linearly dispersing bulk bands into flat Landau levels. In the continuum approximation given by Eq. (4), the bulk spectrum of such Dirac-Landau levels is well known and reads [14]

$$E_n(k_y) = \pm\hbar\sqrt{v_y^2 k_y^2 + 2n v_x v_z \frac{e|B|}{\hbar c}}, \quad n = 1,2,\ldots. \tag{8}$$

The corresponding DOS shows a series of spikes at the onset of each new Landau level and is in a good agreement with the DOS calculated from the lattice model. Deviations occur above ~ 12 meV because the energy dispersion of the lattice model is no longer perfectly linear at higher energies. The peak positions E_n agree perfectly with the Lifshitz-Onsager quantization condition [20], which takes into account these deviations. It requires that $S(E_n) = 2\pi n(eB/\hbar c)$, where $S(E)$ is the extremal cross-sectional area of a surface of constant energy E in the plane perpendicular to $\boldsymbol{B}$ [see Fig. 2(b)], and $n = 1,2,\ldots$.

The pseudomagnetic field $\boldsymbol{b} = \hat{y}b$, induced by strain using Eq. (3) with $u_{33} = 2\alpha x/d$, also generates flat bands [Fig. 3(c)], as expected on the basis of the arguments presented above. The corresponding DOS is in agreement with that obtained from Eq. (8) upon replacing $B \to b$. Remarkably, the agreement is nearly perfect for all energies up to E_{Lif}. We attribute this interesting result to the fact that strain couples as the chiral vector potential *only* to the Weyl fermions. If we write the full Hamiltonian as $h(\boldsymbol{p}) = h_W(\boldsymbol{p}) + \delta h(\boldsymbol{p})$, where h_W is strictly linear in momentum $\boldsymbol{p}$ and δh is the correction resulting from the lattice effects, then strain causes $\boldsymbol{p} \to \boldsymbol{p} - \eta\frac{e}{c}\vec{\mathcal{A}}$ only in h_W but does not to the leading-order affect δh. The real vector potential $\boldsymbol{A}$ affects h_W and δh in the same way.

These results imply that QO will occur when either B or b is present. If we vary B, then $D(E_F)$, together with most measurable quantities, will exhibit oscillations periodic in $1/B$. The same is true for the strain-induced pseudomagnetic field b. This is illustrated in Fig. 4, which shows oscillations in DOS and longitudinal conductivity σ_{yy} at energy 10 meV as a function of $1/b$ and $1/B$. Conductivity is calculated using the standard relaxation time approximation as described in SM.

Strain-induced QOs show robust periodicity in $1/b$. Their period 0.329 T^{-1} is in a good agreement with the period 0.324 T^{-1} expected on the basis of the Lifshitz-Onsager theory and 0.336 T^{-1} obtained from Eq. (8). Small irregularities that appear at low fields can be attributed to the finite size effects as the Landau level spacing becomes comparable to the subband spacing apparent, e.g., in Fig. 3(a). We verified that similar oscillations occur at other energies below the Lifshitz transition. Remarkably, we find strain-induced oscillations periodic in $1/b$ also above E_{Lif}. In addition, we expect that, in

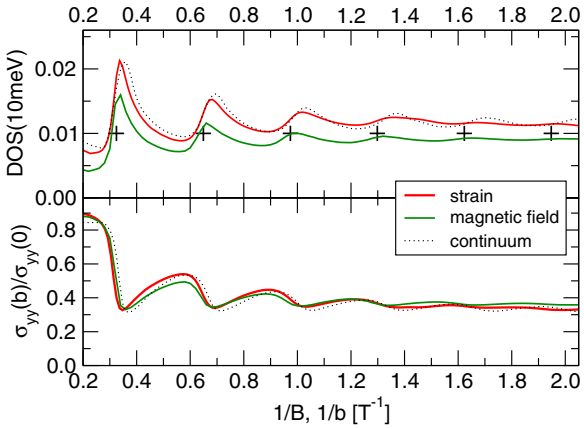

FIG. 4. Strain-induced quantum oscillations. The top panel shows oscillations in DOS at energy 10 meV as a function of inverse strain strength expressed as $1/b$. For comparison, ordinary magnetic oscillations are displayed, as well as the result of the bulk continuum theory Eq. (8). Crosses indicate expected peak positions based on the Lifshitz-Onsager theory. The bottom panel shows oscillations in conductivity σ_{yy} assuming a Fermi energy $E_F = 10$ meV. To simulate the effect of disorder, all data are broadened by convolving in energy with a Lorentzian with width $\delta = 0.25$ meV. The same geometry and parameters are used as in Fig. 3.

the presence of both b and B fields, the peaks split as two Weyl cones feel different effective magnetic fields. These effects are further discussed in SM.

The results presented above extend trivially to the full Cd_3As_2 Hamiltonian Eq. (1), where the spin-down block makes an identical contribution and the p-h symmetry breaking terms contained in ϵ_k bring only quantitative changes (see SM for a discussion). Experimental studies [32–35] indicate that the linear dispersion in Cd_3As_2 extends over a much wider range of energies than theoretically anticipated [31] with the Lifshitz transition occurring near 200 meV. We therefore expect the zero-field strain-induced QO predicted in this work to be easily observable in suitably fabricated Cd_3As_2 films and nanowires and potentially also in other Dirac and Weyl semimetals (see SM for a detailed sketch of the proposed setup). Our results show that conditions for their observability are identical to those required to detect ordinary QO. The continuous tunability of the pseudomagnetic field in a large parameter range provides an experimental basis for the study of emergent gauge fields in three-dimensional crystalline solids.

The authors are indebted to D. A. Bonn, D. M. Broun, A. Chen, I. Elfimov, and W. N. Hardy for illuminating discussions, and thank NSERC, CIfAR, and Max Planck–UBC Centre for Quantum Materials for support.

[1] X. Wan, A. M. Turner, A. Vishwanath, and S. Y. Savrasov, Phys. Rev. B **83**, 205101 (2011).
[2] A. A. Burkov, M. D. Hook, and L. Balents, Phys. Rev. B **84**, 235126 (2011).
[3] O. Vafek and A. Vishwanath, Annu. Rev. Condens. Matter Phys. **5**, 83 (2014).
[4] K. Fukushima, D. E. Kharzeev, and H. J. Warringa, Phys. Rev. D **78**, 074033 (2008).
[5] D. T. Son and B. Z. Spivak, Phys. Rev. B **88**, 104412 (2013).
[6] H.-J. Kim, K.-S. Kim, J.-F. Wang, M. Sasaki, N. Satoh, A. Ohnishi, M. Kitaura, M. Yang, and L. Li, Phys. Rev. Lett. **111**, 246603 (2013).
[7] X. Huang, L. Zhao, Y. Long, P. Wang, D. Chen, Z. Yang, H. Liang, M. Xue, H. Weng, Z. Fang *et al.*, Phys. Rev. X **5**, 031023 (2015).
[8] J. Xiong, S. K. Kushwaha, T. Liang, J. W. Krizan, M. Hirschberger, W. Wang, R. J. Cava, and N. P. Ong, Science **350**, 413 (2015).
[9] A. A. Burkov, J. Phys.: Condens. Matter **27**, 113201 (2015).
[10] Q. Li, D. E. Kharzeev, C. Zhang, Y. Huang, I. Pletikosic, A. V. Fedorov, R. D. Zhong, J. A. Schneeloch, G. D. Gu, and T. Valla, Nat. Phys. **12**, 550 (2016).
[11] C.-L. Zhang, S.-Y. Xu, I. Belopolski, Z. Yuan, Z. Lin, B. Tong, G. Bian, N. Alidoust, C.-C. Lee, S.-M. Huang *et al.*, Nat. Commun. **7**, 10735 (2016).
[12] S. L. Adler, Phys. Rev. **177**, 2426 (1969).
[13] J. S. Bell and R. Jackiw, Nuovo Cimento A **60**, 47 (1969).
[14] H. Nielsen and M. Ninomiya, Phys. Lett. B **130**, 389 (1983).
[15] S. A. Parameswaran, T. Grover, D. A. Abanin, D. A. Pesin, and A. Vishwanath, Phys. Rev. X **4**, 031035 (2014).
[16] Y. Baum, E. Berg, S. A. Parameswaran, and A. Stern, Phys. Rev. X **5**, 041046 (2015).
[17] A. Chen and M. Franz, Phys. Rev. B **93**, 201105 (2016).
[18] A. C. Potter, I. Kimchi, and A. Vishwanath, Nat. Commun. **5**, 5161 (2014).
[19] P. J. W. Moll, N. L. Nair, T. Helm, A. C. Potter, I. Kimchi, A. Vishwanath, and J. G. Analytis, Nature (London) **535**, 266 (2016).
[20] D. Shoenberg, *Magnetic Oscillations in Metals* (Cambridge University Press, Cambridge, UK, 1984).
[21] F. Guinea, M. I. Katsnelson, and A. K. Geim, Nat. Phys. **6**, 30 (2010).
[22] N. Levy, S. A. Burke, K. L. Meaker, M. Panlasigui, A. Zettl, F. Guinea, A. H. C. Neto, and M. F. Crommie, Science **329**, 544 (2010).
[23] H. Shapourian, T. L. Hughes, and S. Ryu, Phys. Rev. B **92**, 165131 (2015).
[24] A. Cortijo, Y. Ferreirós, K. Landsteiner, and M. A. H. Vozmediano, Phys. Rev. Lett. **115**, 177202 (2015).
[25] H. Sumiyoshi and S. Fujimoto, Phys. Rev. Lett. **116**, 166601 (2016).
[26] D. I. Pikulin, A. Chen, and M. Franz, Phys. Rev. X **6**, 041021 (2016).
[27] A. G. Grushin, J. W. F. Venderbos, A. Vishwanath, and R. Ilan, Phys. Rev. X **6**, 041046 (2016).
[28] L. P. He, X. C. Hong, J. K. Dong, J. Pan, Z. Zhang, J. Zhang, and S. Y. Li, Phys. Rev. Lett. **113**, 246402 (2014).
[29] Y. Liu, C. Zhang, X. Yuan, T. Lei, C. Wang, D. Di Sante, A. Narayan, L. He, S. Picozzi, S. Sanvito *et al.*, NPG Asia Mater. **7**, e221 (2015).

[30] J. Xiong, S. Kushwaha, J. Krizan, T. Liang, R. J. Cava, and N. P. Ong, Europhys. Lett. **114**, 27002 (2016).

[31] Z. Wang, H. Weng, Q. Wu, X. Dai, and Z. Fang, Phys. Rev. B **88**, 125427 (2013).

[32] S. Borisenko, Q. Gibson, D. Evtushinsky, V. Zabolotnyy, B. Büchner, and R. J. Cava, Phys. Rev. Lett. **113**, 027603 (2014).

[33] M. Neupane, S.-Y. Xu, R. Sankar, N. Alidoust, G. Bian, C. Liu, I. Belopolski, T.-R. Chang, H.-T. Jeng, H. Lin *et al.*, Nat. Commun. **5**, 4786 (2014).

[34] S. Jeon, B. B. Zhou, A. Gyenis, B. E. Feldman, I. Kimchi, A. C. Potter, Q. D. Gibson, R. J. Cava, A. Vishwanath, and A. Yazdani, Nat. Mater. **13**, 851 (2014).

[35] Z. K. Liu, J. Jiang, B. Zhou, Z. J. Wang, Y. Zhang, H. M. Weng, D. Prabhakaran, S.-K. Mo, H. Peng, P. Dudin *et al.*, Nat. Mater. **13**, 677 (2014).

[36] Z. Wang, Y. Sun, X.-Q. Chen, C. Franchini, G. Xu, H. Weng, X. Dai, and Z. Fang, Phys. Rev. B **85**, 195320 (2012).

[37] Z. K. Liu, B. Zhou, Y. Zhang, Z. J. Wang, H. M. Weng, D. Prabhakaran, S.-K. Mo, Z. X. Shen, Z. Fang, X. Dai *et al.*, Science **343**, 864 (2014).

[38] Y. Zhang, Z. Liu, B. Zhou, Y. Kim, Z. Hussain, Z.-X. Shen, Y. Chen, and S.-K. Mo, Appl. Phys. Lett. **105**, 031901 (2014).

[39] S.-Y. Xu, I. Belopolski, N. Alidoust, M. Neupane, G. Bian, C. Zhang, R. Sankar, G. Chang, Z. Yuan, C.-C. Lee *et al.*, Science **349**, 613 (2015).

[40] B. Q. Lv, H. M. Weng, B. B. Fu, X. P. Wang, H. Miao, J. Ma, P. Richard, X. C. Huang, L. X. Zhao, G. F. Chen *et al.*, Phys. Rev. X **5**, 031013 (2015).

[41] C. Shekhar, A. K. Nayak, Y. Sun, M. Schmidt, M. Nicklas, I. Leermakers, U. Zeitler, Y. Skourski, J. Wosnitza, Z. Liu *et al.*, Nat. Phys. **11**, 645 (2015).

[42] L. X. Yang, Z. K. Liu, Y. Sun, H. Peng, H. F. Yang, T. Zhang, B. Zhou, Y. Zhang, Y. F. Guo, M. Rahn *et al.*, Nat. Phys. **11**, 728 (2015).

[43] S.-Y. Xu, N. Alidoust, I. Belopolski, Z. Yuan, G. Bian, T.-R. Chang, H. Zheng, V. N. Strocov, D. S. Sanchez, G. Chang *et al.*, Nat. Phys. **11**, 748 (2015).

[44] J. Cano, B. Bradlyn, Z. Wang, M. Hirschberger, N. Ong, and B. Bernevig, arXiv:1604.08601.

[45] See Supplemental Material at http://link.aps.org/supplemental/10.1103/PhysRevB.95.041201 for model parameters, low-energy effective theory derivation, conductivity calculation, data on quantum oscillations above the Lifshitz transition, and equivalence of B and b at low energies.

[46] H. Li, H. He, H.-Z. Lu, H. Zhang, H. Liu, R. Ma, Z. Fan, S.-Q. Shen, and J. Wang, Nat. Commun. **7**, 10301 (2016).

[47] C.-Z. Li, L.-X. Wang, H. Liu, J. Wang, Z.-M. Liao, and D.-P. Yu, Nat. Commun. **6**, 10137 (2015).

[48] L.-X. Wang, C.-Z. Li, D.-P. Yu, and Z.-M. Liao, Nat. Commun. **7**, 10769 (2016).